KeAi
CHINESE ROOTS
GLOBAL IMPACT

Contents lists available at ScienceDirect

Petroleum Science

journal homepage: www.keaipublishing.com/en/journals/petroleum-science



Influence of electric and flow field characteristics on the cleaning of fillers for FCCS electrostatic separation



Wei-Wei Xu^a, Can Yang^a, Wei-Lin Yu^b, Zhao-Zeng Liu^a, Qiang Li^{a,*}

- ^a College of New Energy, China University of Petroleum (East China), Qingdao, 266580, Shandong, China
- ^b Daqing Refining and Chemical Company, PetroChina Company Limited, Daqing, 163411, Heilongjiang, China

ARTICLE INFO

Article history: Received 7 December 2024 Received in revised form 30 April 2025 Accepted 19 June 2025 Available online 3 July 2025

Edited by Min Li

Keywords: Fluid catalytic cracking slurry (FCCS) Filler cleaning Particle DC electric field

ABSTRACT

Filler cleaning is a challenge that affects the efficient separation of FCCS particles by electrostatic methods and limits the utilization of the oil slurry. Two filler cleaning methods are proposed in this paper, the flushing desorption method and the electrostatic desorption method, where desorption is achieved by respectively applying a flow field or an electric field to the fillers immersed in a cleaning solution (ethyl acetate). Also, the "rough particle-smooth plane" contact model between particles and filler was established, and the particle force model was established by analyzing the movement of particles in the process of cleaning. Furthermore, combining the established contact model and force model, the detachment model of particles was proposed. In this model, the dimensionless number λ is used to discriminate the attachment state of particles whose validity was verified by experiments. The experimental results showed that the cleaning efficiency of flushing desorption method and electrostatic desorption method increase with the increase of flow rate and voltage, which reached 50.5% and 61.4% at 0.1 m/s and 14 kV.

© 2025 The Authors. Publishing services by Elsevier B.V. on behalf of KeAi Communications Co. Ltd. This is an open access article under the CC BY-NC-ND license (http://creativecommons.org/licenses/by-nc-nd/4.0/).

1. Introduction

Fluid catalytic cracking (FCC) is a crucial process in petroleum refining, involving the thermal cracking of heavy oil with the aid of catalysts to yield cracked gas, gasoline, and diesel. As one of the inevitable by-products, fluid catalytic cracking slurry (FCCS) contains a large amount of aromatic hydrocarbon structures and can be used to produce needle coke, carbon fiber, carbon black, emulsified pitch, and other high-value-added products (Dong et al., 2005; Eser and Wang, 2007; Liu et al., 2022; Nesumi et al., 1990). However, the large amount of catalyst particles contained in FCCS will lead to coking, wear and blockage of the catalytic cracking unit (Song et al., 2018), thereby impeding efficient utilization of FCC slurries.

The methods for removing catalyst particles from FCCS include rotary separation, natural sedimentation, high-temperature filtration and electrostatic separation. Among these methods,

E-mail address: liqiangsydx@163.com (Q. Li).

Peer review under the responsibility of China University of Petroleum (Beijing).

electrostatic separation is widely used in petrochemical, medical and biological fields due to its small pressure drop, high separation efficiency, large processing capacity, and excellent performance in treating small particles (Abd Rahman et al., 2017; Crevillén et al., 2007; Douglas et al., 2017; Freitas et al., 2016; Jesús-Pérez and Lapizco-Encinas, 2011; Mazumder et al., 2006; Sonnenberg et al., 2013). In 1979, Gulf Science Technology Company successfully commercialized an electrostatic separator specifically designed for oil slurries. Fang et al. (1998) conducted an experimental study on the removal of FCCS particles by DEP technology in a transparent electrostatic separator and discovered that the adsorption region of the particles was primarily near the contact point of the filler, proposing the theory of "point adsorption". Li et al. (2020, 2021) investigated the relationship between the angle of the filler contact point and the electric field strength, proposing the "effective contact point" model. Subsequently, they identified an "effective adsorption region" through microscopic experiments and obtained a size model for this region via simulation. Li et al. (2023) then took a series of experiments and found that during the dynamic adsorption process, the overall adsorption efficiency of the device will stabilize over time, implying that the maximum adsorption capacity of the fillers is limited. Experiments and

^{*} Corresponding author.

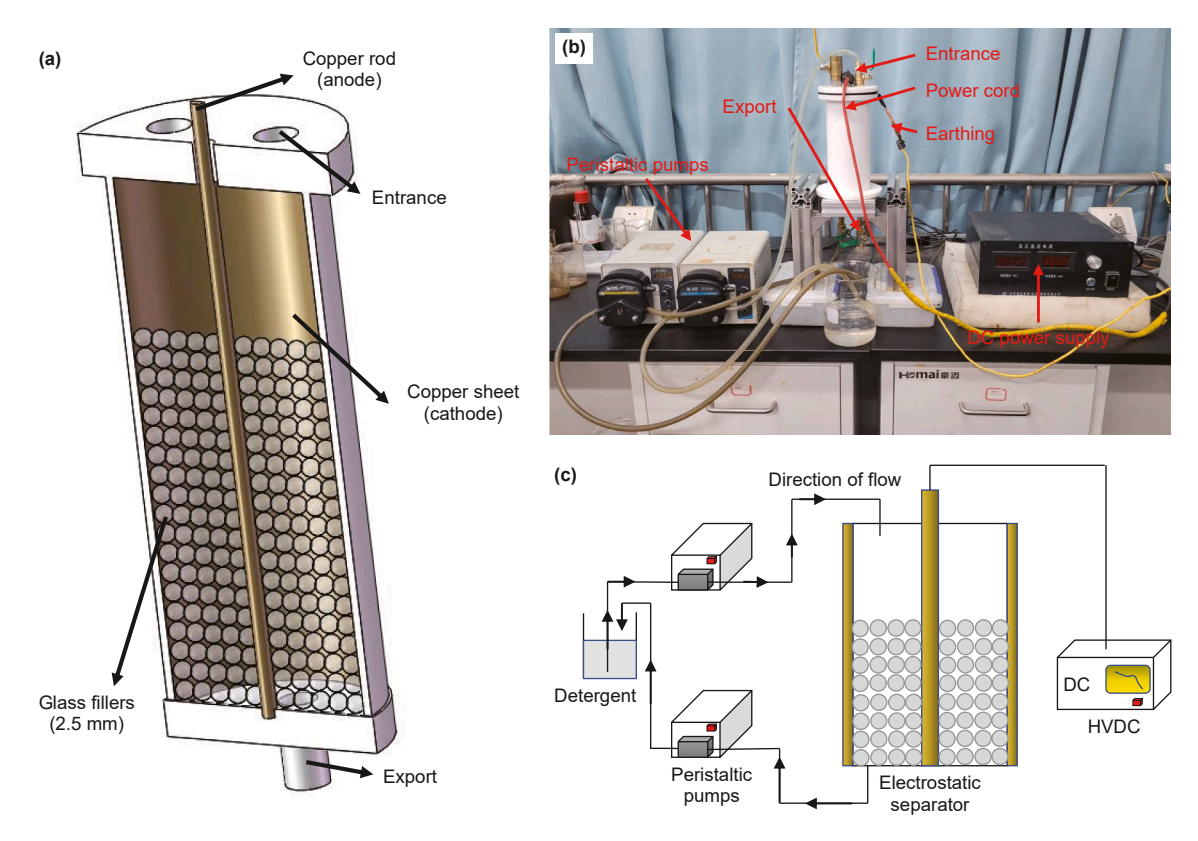


Fig. 1. (a) Electrostatic separator, (b) cleaning experimental setup, (c) schematic diagram.

theories have shown that the available adsorption area of the fillers during the electrostatic adsorption process gradually decreases, therefore, regeneration of the fillers in the electrostatic separator is necessary.

Commonly used filler regeneration methods need to take the filler out of the separator, through high-pressure water rinsing or adding detergent manual cleaning, which significantly increases both the economic and time costs associated with this process. Therefore, it is necessary to find a simple and effective method for filler regeneration. The essence of filler regeneration is the process of catalyst particle detachment from the filler surface. Contact mechanics was first proposed by Hertz, who treated the contact between particles as a static elastic interaction and derived the relationship between the circular contact area and elastic deformation, known as Hertzian theory. Based on Hertzian theory, Johnson et al. (1971) considered the influence of surface energy and surface deformation, connected the contact area with the properties of elastic materials and the strength of surface interaction, and established a model called JKR adhesion theory. Derjaguin et al. (1975), based on Hertzian theory, proposed DMT theory that accounts for deformation calculation, contact area determination, adhesive forces at contacts along with detachment forces caused by Van der Waals forces.

Early studies assumed that both the particle and filler surfaces are smooth, but such surfaces are not perfectly flat. Consequently,

Table 1Catalyst particle parameters.

Average diameter, µm	Mid-diameter, μm	Relative dielectric constant
5.07	3.02	7

numerous studies began to focus on the effect of surface roughness on particle adhesion. Greenwood and Tripp (1967) extended the Hertzian contact model between spheres by considering the degree of surface irregularity. Götzinger and Peukert (2003) took the effect of adsorbed water and surface roughness into account and modeled particle adhesion using a computer-aided empirical potential method. A model for irregular particles consisting of spherical particles and multiple equally-sized smooth hemispherical bumps was developed and employed to investigate the process of particle detachment from surfaces with critical moment analysis and roll detachment theory (Ahmadi and Guo, 2007; Soltani and Ahmadi, 1999). Furthermore, the roughness of the wall surface has been proven to have a significant impact on its adsorption effect in multiple fields, such as the biomedical field (Mu et al., 2023) and the microplastic pollutant treatment industry (Shevchenko et al., 2024).

The different environment in which the particles are located has a great influence on particle desorption. Donald (1969) investigated the impact of external electric fields on adhesion forces and established a strong correlation between these two factors. Rimai and Quesnel (2002) analyzed the influence of electrostatic action on toner adhesion. Berbner and Löffler (1994) found that the Van der Waals force is dominant when in the dry state, while the liquid bridge force is greater than the Van der Waals force in the wet state. Zimon (1982) experimentally found

Table 2 Parameters of ethyl acetate at 25 °C.

Density,	Viscosity,	Conductivity,	Relative dielectric
g/cm ³	mPa·s	S/m	constant
0.902	0.449	$3 imes 10^{-9}$	6

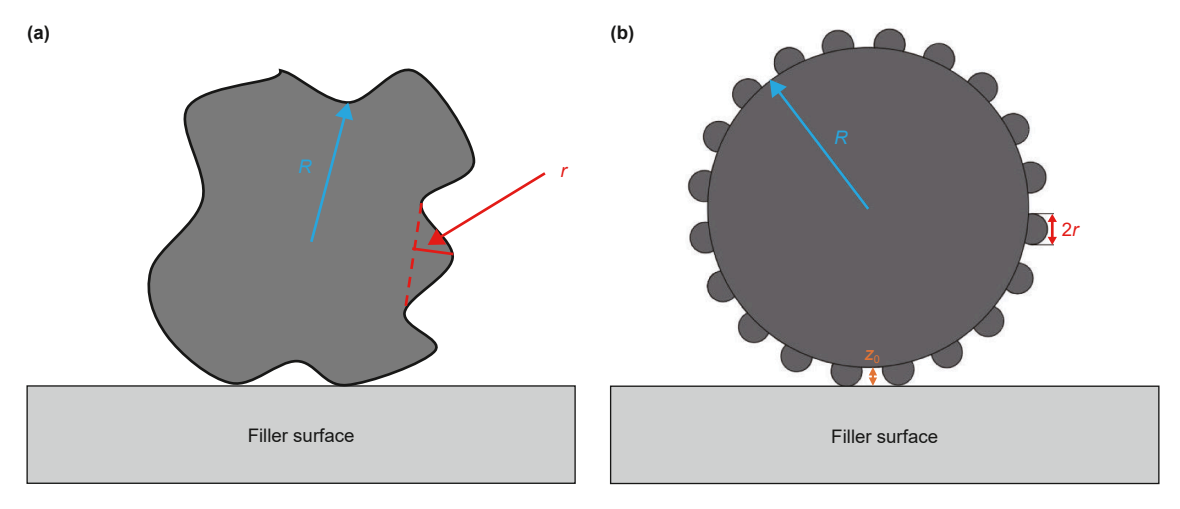


Fig. 2. (a) Schematic diagram of the real contact between rough particles and smooth planes, (b) schematic diagram of the rough particle-smooth plane model.

that the effect of capillary forces is manifested after the particles have been deposited and when the relative humidity of the air is above 65%. Study of Naga et al. (2021) showed that when particles separate from the liquid phase at a liquid-fluid interface, rotation of the particles reduces the force required for separation. Zhou et al. (2023) explored nanoparticle transport in PEBL modified nanopores, proving that environmental factors such as the salt concentration and pH value of the solution in which the particles are located have a relatively significant impact on the movement speed of the particles under the action of an electric field.

Considering the effects of surface roughness and environment on the desorption process, a contact model of rough particle-smooth surface was established to analyze the adsorption and desorption forces on the particles during the processes. These forces were incorporated into the particle force model, and subsequently, a dimensionless equation was developed for judging the desorption by simulation whose feasibility was verified experimentally.

2. Experiment and model description

2.1. Experimental device

Experiments were conducted using a set of devices shown in Fig. 1(a)–(c). The experimental setup primarily consisted of a separator for slurry desolidation and filler cleaning, a high-voltage direct current (HVDC) power supply for providing an adjustable

DC field, and two peristaltic pumps for controlling the flow rate of the cleaning solution. The relative permittivity, conductivity, viscosity, and density are factors that affect the separation efficiency of FCCS during the experiment. It has been experimentally demonstrated that the high viscosity of FCCS at room temperature is not favorable for operation, but that mixing heat transfer oil with a certain mass of catalyst particles at room temperature can more comprehensively reproduce the physical properties of FCCS at high temperature (Zhang et al., 2019). Subsequent experiments would be carried out using the above mixtures, where the parameters of the catalyst particles are presented in Table 1.

The initial step of the experiment was to desolidate the oil slurry to obtain fillers for cleaning purposes. Two regeneration methods, namely flushing and electrostatic desorption, were then employed on the filler to investigate the impact of flow rate and voltage on its regenerative efficacy. The cleaning reagent used in the experiments was ethyl acetate, which has excellent fluidity and solubility for oil slurries. The parameters are shown in Table 2.

The filler cleaning efficiency is calculated by the mass method with the following formula:

$$\eta = \frac{m''}{(m-m')} \tag{1}$$

where, η is the cleaning efficiency, m is the catalyst mass in the thermal fluid before electrostatic separation, m' is the catalyst mass in the thermal fluid after electrostatic separation, and m'' is the catalyst mass in the cleaning reagent after cleaning.

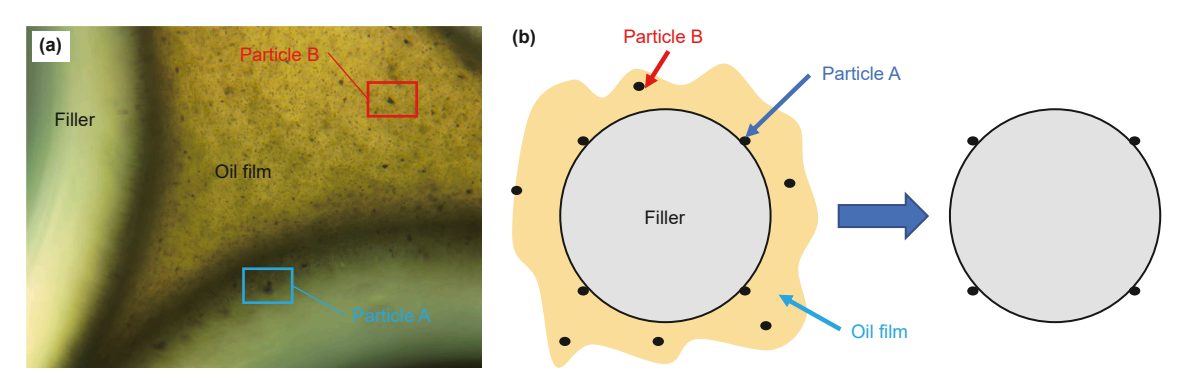


Fig. 3. (a) Scheme of oil film between fillers, (b) filler before and after removal of oil film.

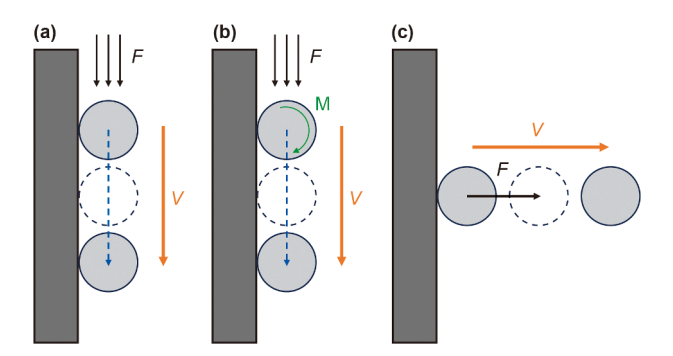


Fig. 4. Particle desorption form: (a) sliding, (b) rolling, (c) lifting.

2.2. Particle desorption model and discriminants

The adhesion and detachment behavior of particles are primarily caused by the changes in forces. Resuspension is a complex process influenced by both aggregation forces (which promote particle adhesion to object surfaces) and dispersal forces (which facilitate particle detachment from object surfaces). In this study, ignoring the interaction force between the particles under the low solid concentration condition, the forces acting on the particles can be divided into two categories: dispersing forces arising from the electric field, flow field, and gravity field; and aggregation forces generated by residual FCCS coverage on the filler surface. The dispersal forces include dielectrophoretic, drag, pressure gradient, Saffman lift, buoyancy, and gravity, while the aggregation forces encompass Van der Waals and surface tension.

2.2.1. Particle force model

In the Cartesian coordinate system, the momentum equation of particle motion is shown in Eq. (2):

$$m_{\rm p} \frac{\mathrm{d}u_{\rm j}}{\mathrm{d}t} = \sum F_{\rm j} \tag{2}$$

where, m_p is the mass of catalyst particles, u_j is the velocity of particles in j direction, and ΣF_j is the resultant force of particles in j direction.

Under the electric field, the dielectrophoresis force of the catalyst particles can be obtained using the following equation:

$$F_{\rm DEP} = \frac{\pi}{4} d_{\rm p}^3 \varepsilon_0 \frac{\varepsilon_{\rm r,f}^* \left(\varepsilon_{\rm r,p}^* - \varepsilon_{\rm r,f}^*\right)}{\varepsilon_{\rm r,p}^* + 2\varepsilon_{\rm r,f}^*} \tilde{N} |E_{\rm rms}|^2$$
 (3)

where, $d_{\rm p}$ indicates the particle diameter; ε_0 is the absolute permittivity, $\varepsilon_{\rm r,f}^*$ and $\varepsilon_{\rm r,p}^*$ are the complex relative permittivity of the fluid and particles; $E_{\rm rms}$ indicates the root mean square value of the electric field intensity; since the power supply used is HVDC power, $E_{\rm rms} = E$, $\varepsilon_{\rm r}^* = \varepsilon_{\rm r}$.

The buoyant force and the gravitational force acting on the particles in liquid medium are in opposite directions, necessitating the replacement of these two forces with a single force known as effective gravity, as demonstrated by Eq. (4):

$$F_{\rm EG} = m_{\rm p} g \frac{\rho_{\rm p} - \rho_{\rm f}}{a} \tag{4}$$

where, $m_{\rm p}$ is the particle mass, g is the gravity acceleration, $\rho_{\rm p}$ and $\rho_{\rm f}$ are the density of the particle and the fluid media.

In the flow field, when the particles are in relative motion with the fluid, the particles will be affected by the drag force from the fluid. The expression for the drag force is shown in Eq. (5):

$$F_{SD} = \frac{1}{\tau_p} m_p(\boldsymbol{u} - \boldsymbol{v}) = 3\pi\mu d_p(\boldsymbol{u} - \boldsymbol{v})$$
 (5)

where, \boldsymbol{u} and \boldsymbol{v} indicate the velocity of the particles and the fluid, $\tau_{\rm p}$ is the velocity response time of particles. The fluid velocity in this study is characterized by a low Reynolds number, indicating that it falls within the regime of Stokes flow, so $\tau_{\rm p} = 2\rho_{\rm p} r_{\rm p}^2/9\mu$, where $r_{\rm p}$ is the particle radius and μ is the fluid viscosity.

If there is a pressure gradient in the flow field, the particles will be subjected to the pressure gradient force as shown in Eq. (6):

$$F_{\rm p} = -\frac{\pi d_{\rm p}^3}{6} \frac{\partial P}{\partial l} \tag{6}$$

where, $\partial P/\partial I$ indicates the pressure gradient along the direction of the flow.

Due to the existence of a velocity gradient in the nearby flow field, particles will be affected by the Saffman lift force. The Saffman lift force is calculated by Eq. (7):

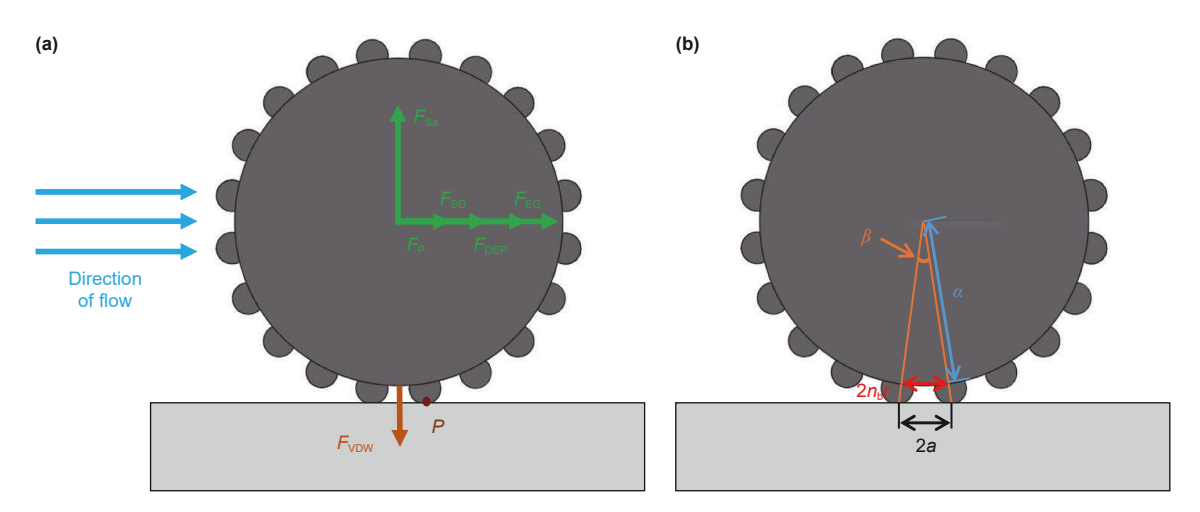


Fig. 5. (a) Particle force diagram where the green force represents the dispersal force while the brown is the aggregation force, (b) rolling point location.

$$F_{Sa} = -1.615 d_p^2 \rho_f \left(u_p - u_f \right) \sqrt{\nu \left(du_f / dy \right)}$$
 (7)

where, $\rho_{\rm f}$ is the viscosity of fluid motion, ${\rm d}u_{\rm f}/{\rm d}y$ is the fluid velocity gradient.

Since the Van der Waals force is the main determining force for particle adhesion to the filler surface and this force is mainly affected by the surface shape of the catalyst particle, for the convenience of study, the surface of the filler is regarded as relatively smooth surface, while the surface of the particle is considered to be rough surface consisting of a number of spheres. The radius of the spheres is calculated by Eq. (8) (Picotti et al., 2018):

$$r = \frac{2R}{n_{\rm u}n_{\rm b}\sqrt{N}}\tag{8}$$

where, R and r are the radii of the particle and radii of the sphere on the particle surface, $n_{\rm u}$ is a parameter greater than 1 to control the unevenness of the distribution of surface bumps(when $n_{\rm u}=1$ is regarded as the average distribution), $n_{\rm b}$ ($n_{\rm b}=1,2,3\cdots$) controls the average spacing between the bumps in contact with the substrate (the distance between the center of mass of the contacting convex element and the base is $2n_{\rm b}r$, and the distance between the center of mass of the non-contacting convex element is $2n_{\rm u}n_{\rm b}r$), and N is the number of bumps.

In this study, supposing that the number of rough bumps on the surface of catalyst particles N=20 and the bumps are evenly distributed, so that $n_{\rm u}=1$ and the average spacing between the bumps in contact with the substrate $n_{\rm h}=2$.

The rough particle-smooth surface is shown in Fig. 2 and the Van der Waals forces can be calculated by Eq. (9):

$$F_{\text{VDW}} = \frac{A_{\text{Ham}}}{6} \left[\frac{r}{z_0^2} + \frac{R}{(z_0 + r)^2} \right]$$
 (9)

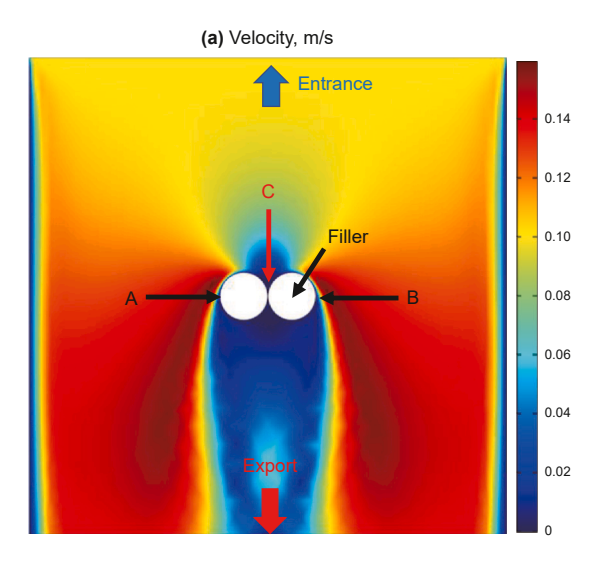
where, $A_{\rm Ham}$ is the Hamaker constant of particles, R is the radius of the particle, and r is the radius of the convex surface of particle; z_0 indicates the distance of the particle from the surface.

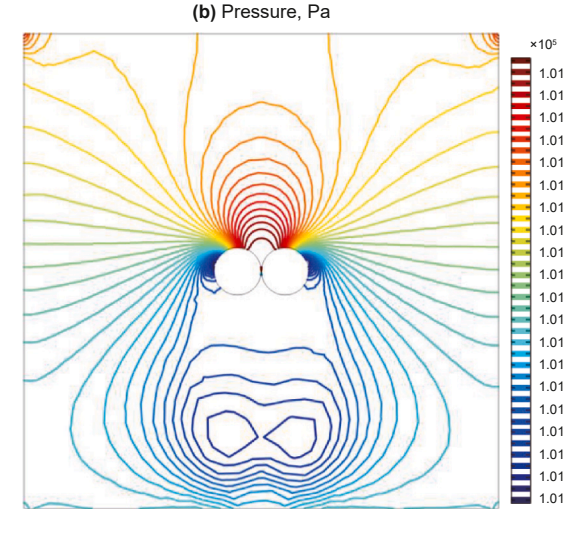
As shown in Fig. 3(a), after the electrostatic adsorption is completed, the oil slurry is discharged, leaving an oil film on the surface of the filler due to its interaction with surface tension. At this time, the particles are wrapped in the oil film and bound by the surface tension. Two types of particles can be observed: Particle A is adsorbed on the surface of the filler, and Particle B is attached to the oil film. In this study, the surface tension coefficient of heat transfer oil in air is 36.6 dyn/cm, thus the surface tension acting on the particles from the oil (approximately $10^{-7}\,\mathrm{N})$ is much greater than the particle's gravity (approximately 10^{-13} N) and other decoupling forces. In other words, the existence of the oil film greatly affects the process of particle detachment. The cleaning media selected in the experiment exhibits excellent solubility to the heat transfer oil, preventing the negative effect of oil film on cleaning, as shown in Fig. 3(b). Particle B is removed along with the oil film while Particle A avoids being affected by surface tension and can be more easily desorbed.

2.2.2. Desorption model

The desorption of particles is classified into three types based on the equilibrium between forces and moments acting on them: sliding, rolling, and lifting, as illustrated in Fig. 4. Sliding refers to the movement of the particle along the filler surface under the influence of external forces, rolling denotes the rotational motion of particles on the surface of an object when the equilibrium state of moments is disrupted, lifting represents the upward motion perpendicular to the surface due to the lift force. The three types of

desorption do not occur individually but manifest multiple forms with the increase of particle size. When the particle size is greater than 1.6 μm , the desorption form of particles exhibits rolling, and





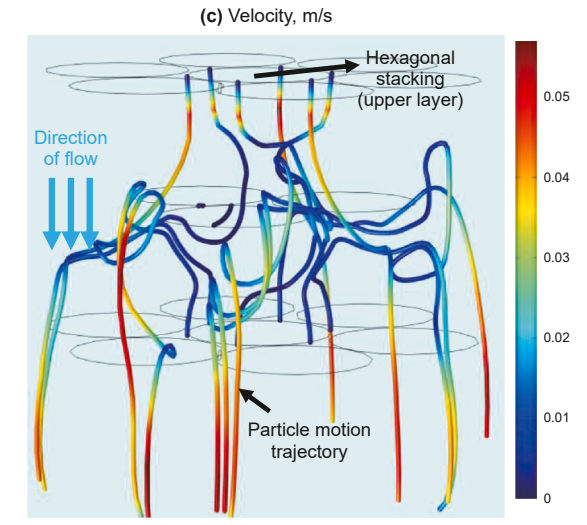


Fig. 6. Flow field **(a)**, pressure diagrams **(b)**, and particle trajectory **(c)** at an inlet velocity of 0.1 m/s.

when the particle size is further larger than 80 μ m, the desorption form will show sliding and rolling (Zoeteweij et al., 2009). As shown in Table 1, the average particle size of catalyst particles in this study is 5 μ m, so the research will focus on the rolling motion process of particles.

The occurrence of particle rolling needs to be determined based on the state of moment equilibrium. If the moment generated by the aggregation force exceeds that generated by the dispersal force, the particle will roll under this influence; however, if the moment generated by the aggregation force is less than that generated by the dispersal force, the particle will not. The research was divided into two parts, electrostatic desorption and flushing desorption, depending on the desorption method used. The repulsion forces on the particles under the two methods are different, and the force analysis diagrams and rolling point locations are shown in Fig. 5. For each of the two desorption methods, a judgment equation and a dimensionless constant λ were proposed. When $\lambda \geq 1$, the particle can achieve desorption; when $\lambda < 1$, the particle fails to desorb and remains adsorbed on the filler surface.

The dispersal forces of flushing desorption method include Saffman lift force F_{Sa} , pressure gradient F_{P} , drag force F_{SD} , and effective gravity F_{EG} . Detachment discriminant for flushing desorption method and dimensionless number λ_1 are shown as:

$$(F_{P} + F_{SD} + F_{EG}) \cdot a / \tan(\beta / 2) + F_{Sa} \cdot a \ge F_{VDW} \cdot a$$

$$\tag{10}$$

$$\lambda_1 = \frac{F_P + F_{SD} + F_{EG} + F_{Sa} \cdot \tan(\beta/2)}{F_{VDW} \cdot \tan(\beta/2)}$$
(11)

The dispersal forces of electrostatic desorption method include dielectrophoretic force $F_{\rm DEP}$ and effective gravity $F_{\rm EG}$. Detachment discriminant for electrostatic desorption method and dimensionless number λ_2 are:

$$(F_{\text{DEP}} + F_{\text{EG}}) \cdot a / \tan(\beta / 2) \ge F_{\text{VDW}} \cdot a \tag{12}$$

$$\lambda_2 = \frac{F_{\text{DEP}} + F_{\text{EG}}}{F_{\text{VDW}} \cdot \tan(\beta/2)} \tag{13}$$

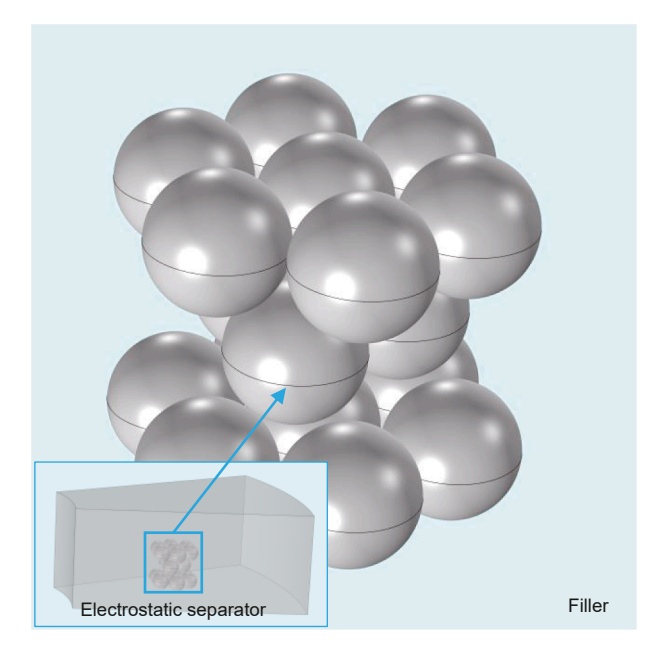
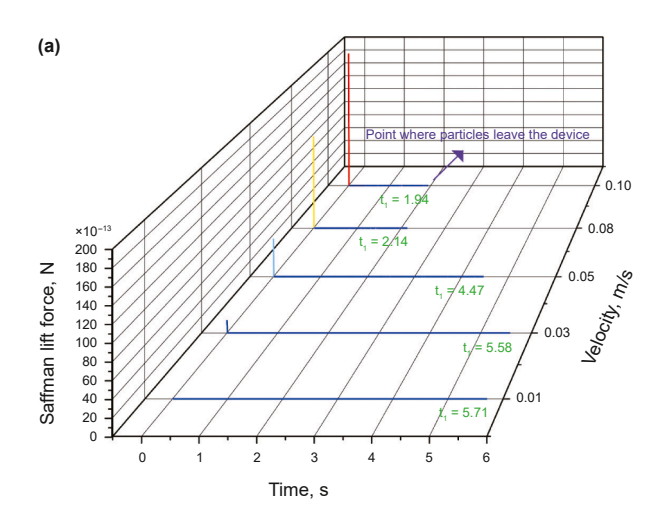


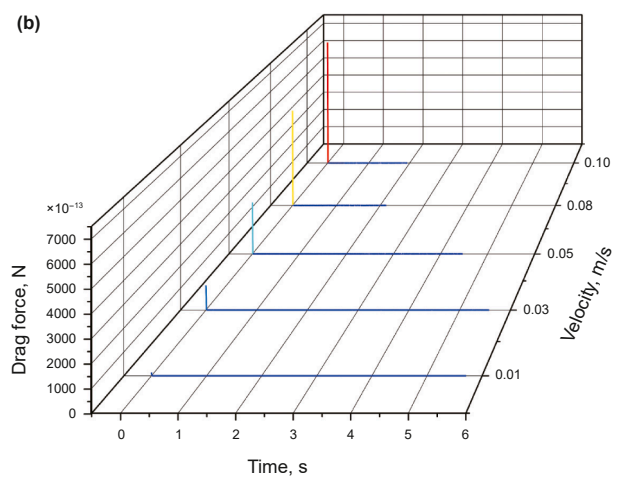
Fig. 7. Electrostatic separator model and filler hexagonal densest stacking model.

3. Results and analysis

3.1. The effect of flow velocity on cleaning efficiency

The fillers in the electrostatic separator typically exhibit irregular accumulation. When the cleaning solution flows through the fillers, the flow field induces drag force, pressure gradient force and Saffman lift force to facilitate particle desorption. However,





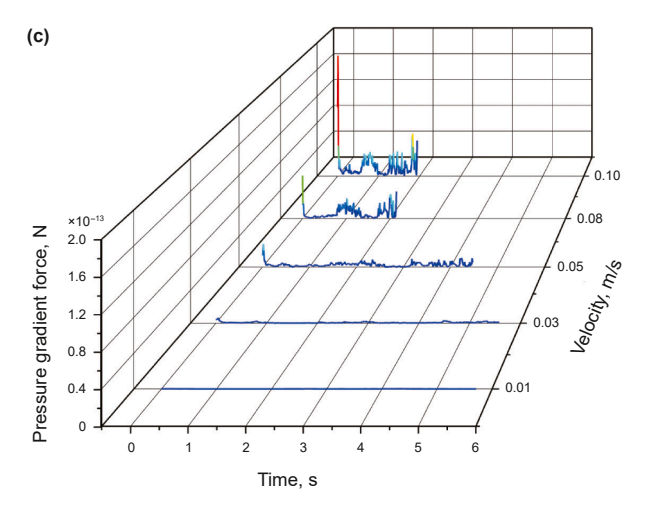


Fig. 8. Variation of flow field force at different flow velocities: **(a)** Saffman lift force, **(b)** drag force, **(c)** pressure gradient force.

Table 3 Flow field forces at the initial time.

Velocity, m/s	F _{Sa} , N	F _{SD} , N	F _P , N
0.01	7.78×10^{-14}	1.44×10^{-11}	9.82×10^{-17}
0.03	1.57×10^{-12}	1.13×10^{-10}	4.39×10^{-15}
0.05	4.97×10^{-12}	2.53×10^{-10}	1.66×10^{-14}
0.08	1.29×10^{-11}	4.99×10^{-10}	6.03×10^{-14}
0.10	1.98×10^{-11}	6.79×10^{-10}	1.03×10^{-13}

due to the complex stacking structure of the fillers, the characteristics of the flow field undergo complex changes, which consequently alters the forces generated within it. The flow field characteristics of the cleaning solution as it flows through the fillers will be analyzed below to investigate the flow field forces on the particles at different flow rates and the link between λ and cleaning efficiency.

Due to the significant size differences between particles and fillers, the effect of the particles on the flow field characteristics was neglected, so a two-sphere model was used to represent fillers with particles absorbed. When the cleaning solution flew over the surface of the fillers, a separation of the boundary layer occurred, as shown in Fig. 6. It was evident that high velocity, velocity gradient, and pressure gradient near the outer side of the fillers (A and B) resulted in maximum trailing forces, lift forces, and pressure gradient forces acting upon particles on this side, facilitating desorption. Conversely, the velocity gradient and pressure gradient generated near the inner side of the fillers (C) were in the opposite direction to the flow, and the velocity was extremely low, which caused the inner particles to move in the direction opposite to that of the outer particles.

In conclusion, the particles on the outer side of the filler are easier to achieve desorption, while the inner particles move in the opposite direction of the outer particles and are subjected to a quite small drag force, which makes it more difficult to achieve desorption.

To facilitate calculations and better guide the placement of fillers in the separator, a model was established, as shown in Fig. 7, including a portion of the electrostatic separator and a hexagonal densest stacking arrangement of the fillers. The particle trajectory during the desorption process was simulated by the particle tracking module of COMSOL Multiphysics software, where the cleaning solution entered from above and flew out from the bottom. The initial release position of the particle was the contact point between the fillers in the hexagonal densest stacking model. The obtained particle motion trajectory is shown in Fig. 6(c), indicating that the particles near the upper filler layer moved in the same direction as the cleaning solution flow, while those near the lower filler layer moved in the opposite direction. It can be observed that when both particles were horizontally positioned at point C shown in Fig. 6(a) and vertically located in the upper and lower filler layers, respectively, both the Saffman lift force and the pressure gradient force on the two particles were opposite. Furthermore, as shown in Fig. 6(c), the particles close to the lower filler layer moved at a lower speed than those near the upper layer.

Table 4 Dimensionless numbers λ_1 .

Velocity, m/s	λ_1
0.01	135.3
0.03	1057.3
0.05	2372.5
0.08	4692.8
0.10	6395.7

It can be concluded that in the actual flushing process, as the number of filler layers increases, the cleaning effect of the fillers gradually worsens. Therefore, to ensure cleaning efficiency during the flushing process, it is advisable to minimize the number of filler layers. In cases where a large quantity of fillers needs to be cleaned, increasing the diameter of the cleaning device may be considered as a means to reduce the number of filler layers and maintain optimal cleaning performance.

Fig. 8 shows the variation of the force at different flow velocities obtained from the simulation. Specifically, the total length of the force curve decreased as the flow rate increased, which resulted from the increase in particle velocity that reduced the time for particles to disengage from the device. During the early stages of particle separation, when particles were still within the fillers' area, detachment occurred due to a combination of pressure gradient force, lift force, and drag force. However, as particles left this area, both fluid velocity and velocity gradients decayed rapidly, leading to a significant decrease in drag force and Saffman lift forces. Once the velocity returned to the inlet flow rate, the particles were subjected to the flow field force only by the drag force.

Therefore, it can be deduced that, on the one hand, among the forces on the particle in a flow field, the pressure gradient force, lift force, and drag force determine whether the particle can leave the surface of the fillers. On the other hand, the motion of the particle is determined solely by the drag force when the particle leaves the vicinity of the fillers. Thus, it is feasible to determine whether desorption of a particular particle can be achieved at different flow rates by analyzing the forces acting on the particle. Specifically, by extracting the pressure gradient force, lift force, and drag force on a particle at the initial time, λ_1 can be calculated by Eq. (11) to determine whether the particle can achieve desorption.

Table 3 shows the magnitude of flow field forces acting on the particle at various flow velocities. By substituting the flow field forces into Eq. (11), the dimensionless number λ_1 for different flow velocities can be obtained, as is presented in Table 4.

The results presented in Table 4 demonstrate that λ_1 consistently exceeded 1 across various flow rates, suggesting complete desorption of particles. It can be observed that the dimensionless number λ_1 monotonically increased with flow rate, indicating that higher flow rates facilitate easier particle desorption and enhance cleaning efficiency.

A quadratic polynomial was fitted between λ_1 and velocity, given by Eq. (14) using data from Table 4:

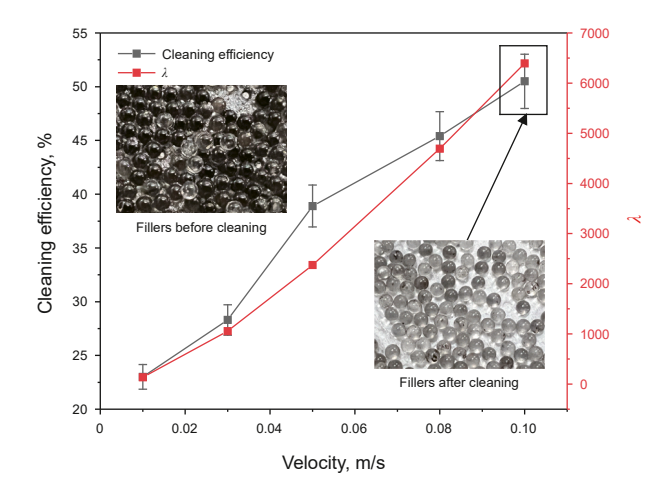


Fig. 9. Cleaning efficiency and λ obtained from experiments at different flow rates (with comparison of fillers before and after cleaning at velocity of 0.1 m/s).

$$\lambda_1 = 274084.85v^2 + 40148.93v - 328.20 \tag{14}$$

where, v indicates the velocity of fluid flow. Verification showed that, within the data range, the estimated λ_1 values differ from the calculated λ_1 values by less than 1% error.

Utilizing the experimental setup shown in Fig. 1, the experimental results obtained are shown in Fig. 9. It can be observed that the cleaning efficiency steadily increased with the flow rate, which is consistent with the results obtained from the simulation.

3.2. The effect of voltage on cleaning efficiency

During the purification process of oil slurry, polarization occurs near the fillers due to the influence of an electric field, resulting in particles being attracted to the vicinity of fillers and adsorbed onto the surface of fillers by dielectrophoretic force. The extent of polarization depends on both the relative dielectric constant of the fillers and the liquid phase medium. When the relative dielectric constant of the liquid phase medium exceeds that of the fillers, the electric field strength near the contact point of the fillers is weakened. Conversely, when the relative dielectric constant of the liquid phase medium is lower than that of the fillers, the electric field strength near the contact point is enhanced. Therefore, when replacing the liquid phase medium with different dielectric constants, the effect of the dielectrophoretic force acting on the particles alters.

As shown in Fig. 10(b), when oil slurry was used as a liquid phase medium, the electric field strength in the contact area of the fillers was stronger than in other areas, causing the particles to be adsorbed onto the surface of the fillers by the dielectrophoretic force directed toward the contact point of the fillers. Conversely, as illustrated in Fig. 10(a), when the oil slurry was replaced with ethyl acetate, the electric field strength in the contact area of the fillers weakened compared to other areas, driving the particles to detach from the surface of the fillers due to the dielectrophoretic force

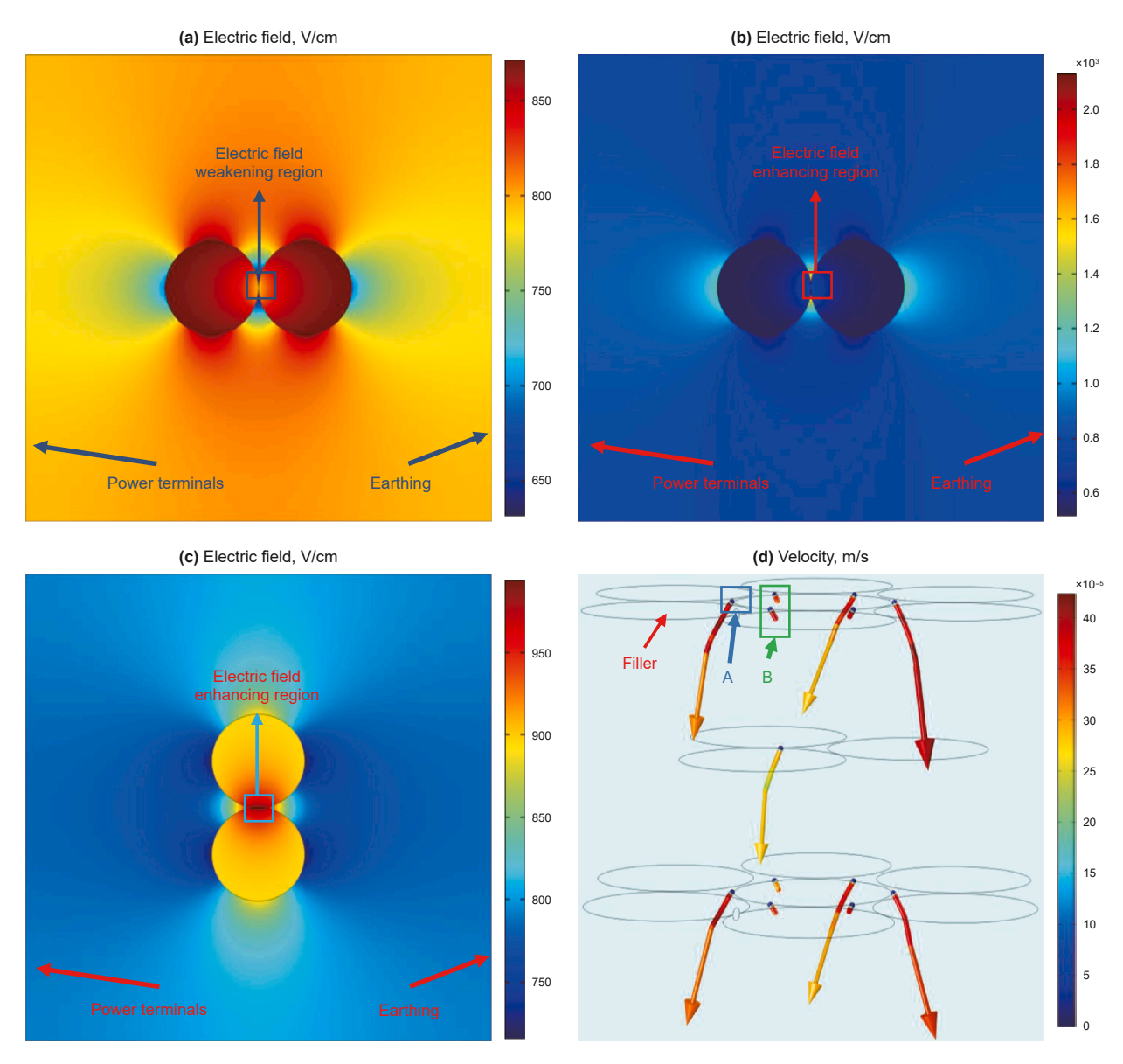


Fig. 10. Electric field intensity near the paired fillers (a) in ethyl acetate at clamping angle of 0°, (b) in oil slurry at 0° and (c) in ethyl acetate at 90°; (d) trajectory of particles at voltage of 14 kV.

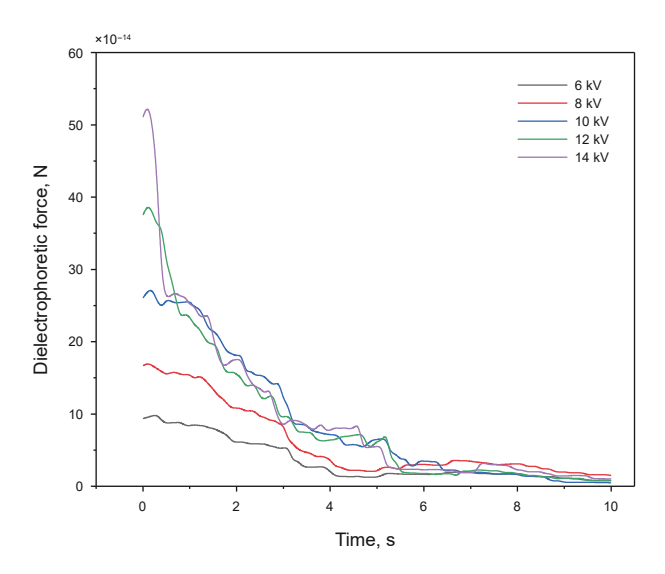


Fig. 11. Dielectrophoretic force at different voltages.

Table 5 Dielectrophoretic force and λ_2 of the initial position at different voltages.

Voltage, kV	F_{DEP} , N	λ_2
6	9.38×10^{-14}	2.126
8	1.68×10^{-13}	2.815
10	2.61×10^{-13}	3.678
12	3.75×10^{-13}	4.736
14	5.11×10^{-13}	5.998

directed away from the contact point, thereby allowing for the cleaning of the fillers.

The simulation model employed in this study is consistent with the hexagonal densest stacking model depicted in Fig. 7, and the particle trajectory diagram resulting from voltage application is illustrated in Fig. 10(d). It can be observed that some particles were successfully detached from the filler surface (e.g., A), while others exhibited relatively slow or even stationary movement (e.g., B). At contact points A and B of the fillers, the different angles between

the center-of-mass lines of the two contacting fillers and the electric field lines resulted in varying polarization degrees at these locations, which caused different dielectrophoretic forces acting on particles located at those points. In an ethyl acetate medium, specifically, the electric field strength at the filler contact point weakened when the angle was 0° , while it strengthened when the angle was 90° , as shown in Fig. 10(c). In fact, based on the electric field distribution shown in Fig. 10(a), most particles were absorbed in the vicinity of point A in Fig. 10(d) before the desolidation process. It can be assumed that the particles near point B have a negligible effect on the analysis of the effectiveness of the electrostatic desorption method.

Fig. 11 shows the curves of dielectrophoretic force over time at different voltages. It is evident that an increase in voltage led to a steeper decline in dielectrophoretic force. This occurred because higher voltages resulted in greater dielectrophoretic force acting on particles at their initial positions, allowing them to exit the polarization region more rapidly and consequently producing a larger slope on the curve under high voltage conditions.

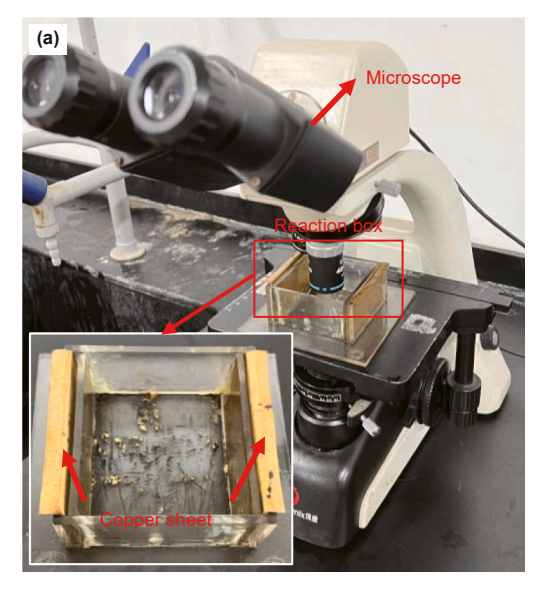
To directly assess whether the particles can be desorbed under the electric field, the dielectrophoretic forces at the starting position under different voltages were extracted and substituted into Eq. (13) to calculate the dimensionless number λ_2 . The extracted dielectrophoretic forces and their λ_2 values are shown in Table 5. It was found that the values of λ_2 at all voltages were larger than 1 and increased with voltage, indicating that the particles can achieve desorption at these voltages, and the higher the voltage the better the desorption effect.

A quadratic polynomial was fitted between λ_2 and voltage, given by Eq. (15) using data from Table 5:

$$\lambda_2 = 0.02395V^2 + 0.00432V - 1.24117 \tag{15}$$

where, V indicates the voltage applied across the fluid domain. Within the data range, the estimated λ_2 values were verified to be less than 1% in error compared to the calculated λ_2 values.

To visually depict the motion of catalyst particles during electrostatic desorption, microscopic desorption experiments were conducted using electron microscopy to observe particle movement under an electric field. The experimental setup is illustrated in Fig. 12(a). The main body of the device is made of Plexiglas, with



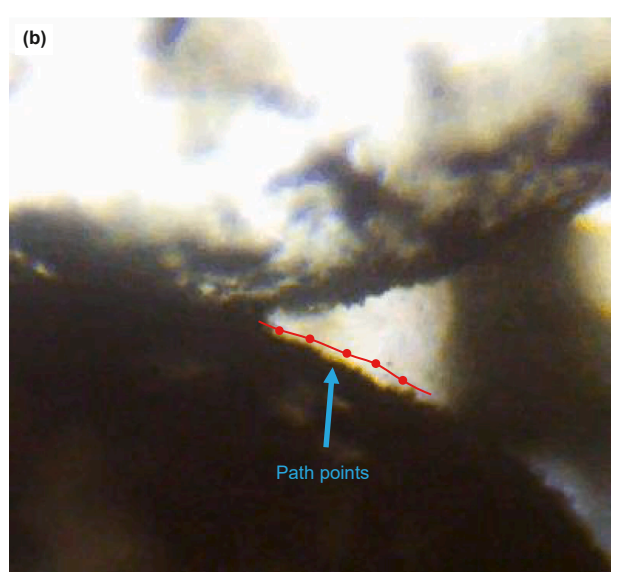


Fig. 12. (a) Electrostatic desorption microscopic experimental device, (b) particle motion trajectory diagram.

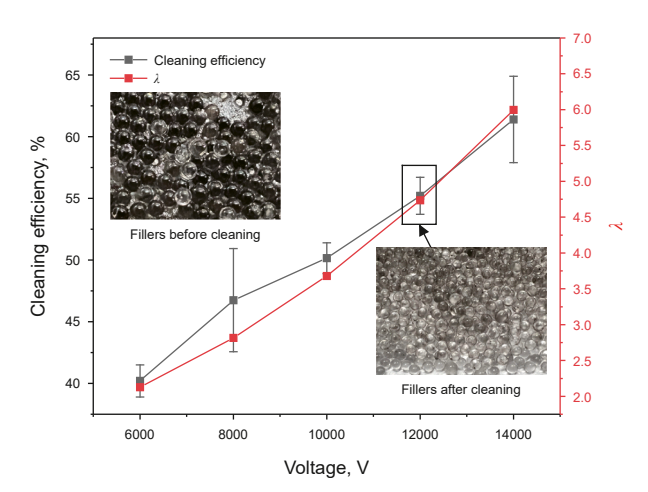


Fig. 13. Cleaning efficiency and λ obtained from experiments at different voltages (with comparison of fillers before and after cleaning at voltage of 12 kV).

two copper electrodes positioned on either side and a square area in the center for placing the fillers to be cleaned. It should be noted that, due to its smaller size compared to the electrostatic separator, the microscopic experimental device generated a higher electric field strength at the same voltage. The desorption process of the particles was observed at 2000 V, and particle motion was recorded over a period of 30 min. A clear particle trajectory was then selected for analysis, with data points captured every 2 s, as shown in Fig. 12(b). Under the applied electric field, the particles gradually moved away from the filler contact point due to the dielectrophoretic force and achieved desorption.

By introducing the electrostatic desorption agent ethyl acetate and applying varying voltages, a comparative graph illustrating the cleaning efficiency of the fillers was obtained, as depicted in Fig. 13. The graph clearly demonstrated a gradual increase in cleaning efficiency with increasing voltage, which aligned with the observed trend of λ_2 and verified the accuracy of the dimensionless number λ_2 .

4. Conclusion

Based on the analysis of particle adhesion and detachment mechanism, numerical simulations combined with experimental methods were employed to investigate the cleaning of fillers, with a focus on the effects of flow field characteristics (flow velocity) and electric field characteristics (voltage) on cleaning efficiency. The main conclusions are as follows:

- (1) The forces acting on catalyst particles during the filler cleaning process were analyzed, and a rough particlesmooth plane model was established as the contact model of the particles based on the surface physical properties of both the fillers and the particles.
- (2) Two desorption discriminant dimensionless numbers λ_1 and λ_2 were proposed for different cleaning methods, expressed

as
$$\begin{cases} \lambda_1 = \frac{F_{\rm DEP} + F_{\rm EG}}{F_{\rm VDW} \cdot \tan(\beta/2)} \\ \lambda_2 = \frac{F_{\rm P} + F_{\rm SD} + F_{\rm EG} + F_{\rm Sa} \cdot \tan(\beta/2)}{F_{\rm VDW} \cdot \tan(\beta/2)} \end{cases}$$
, indicating that the

particle desorption behavior is mainly determined by the forces acting on the particles and the rolling desorption model. The feasibility of the discriminants was verified through experiments and simulations.

(3) The effects of varying flow rates of the cleaning solution and voltage on the cleaning efficiency were investigated, revealing a positive correlation between increased flow rate and voltage with enhanced cleaning performance. Specifically, when the flow rate was increased from 0.01 to 0.1 m/s using the flushing desorption method, the cleaning efficiency improved significantly from 23% to 50.5%. Similarly, by increasing the voltage from 6 to 14 kV employing the electrostatic desorption method, a notable enhancement in cleaning efficiency was observed, rising from 40.2% to 61.4%.

The Lagrangian method, which is suitable for sparse flow (such as the mass of catalyst particles in this paper accounting for less than 1% of the two-phase flow), was used to discuss the electrostatically induced movement of particles in the oil phase in this paper. This method ignores the influence of solid particles on fluid flow and is more efficient in the overall study of forces and the tracking of particle trajectories. In catalyst particles, individuals with a spherical or nearly spherical shape occupy the majority. However, a considerable part of the catalyst particles is also with sharp depressions or protrusions, or even completely irregular shapes. The existence form of this catalyst particle will significantly affect the DEP force and various hydrodynamic forces mentioned in the paper. Studies have shown that interactions between the particles under investigation (Zhou et al., 2020a), particle size (Zhou et al., 2020b), and other factors significantly affect particle velocity. Building upon the research in this paper, the morphology of particles can be further investigated at the catalyst particle scale (several or tens of micrometers). In such cases, the Arbitrary Lagrangian-Eulerian (ALE) method (Zhou et al., 2023) can be used to describe the motion of particles and fluid flow in fluid-solid coupling system. This is also an important step for the electrostatic de-solidification of catalytic cracking slurry and filler cleaning towards research at a smaller scale.

CRediT authorship contribution statement

Wei-Wei Xu: Writing – review & editing, Writing – original draft, Supervision, Resources, Funding acquisition, Formal analysis, Conceptualization. **Can Yang:** Writing – review & editing, Writing – original draft, Validation, Investigation, Formal analysis, Conceptualization. **Wei-Lin Yu:** Writing – review & editing, Validation, Investigation. **Zhao-Zeng Liu:** Writing – review & editing, Software, Conceptualization. **Qiang Li:** Writing – review & editing, Funding acquisition, Formal analysis.

Declaration of competing interest

The authors declare that they have no known competing financial interests or personal relationships that could have appeared to influence the work reported in this paper.

Acknowledgements

This research is funded by the National Natural Science foundation of China (No. 52476043).

References

Abd Rahman, N., Ibrahim, F., Yafouz, B., 2017. Dielectrophoresis for biomedical sciences applications: a review. Sensors 17 (3), 449. https://doi.org/10.3390/s17030449.

- Ahmadi, G., Guo, S., 2007. Bumpy particle adhesion and removal in turbulent flows including electrostatic and capillary forces. J. Adhes. 83 (3), 289–311. https://doi.org/10.1080/00218460701239174.
- Berbner, S., Löffler, F., 1994. Influence of high temperatures on particle adhesion.

 Powder Technol. 78 (3), 273–280. https://doi.org/10.1016/0032-5910(93)
 02798-F.
- Crevillén, A.G., Hervás, M., López, M.A., et al., 2007. Real sample analysis on microfluidic devices. Talanta 74 (3), 342–357. https://doi.org/10.1016/j.talanta.2007.10.019.
- Derjaguin, B.V., Muller, V.M., Toporov, Y.P., 1975. Effect of contact deformations on the adhesion of particles. J. Colloid Interface Sci. 53 (2), 314–326. https://doi.org/10.1016/0021-9797(75)90018-1.
- Donald, D.K., 1969. Electrostatic contribution to powder-particle adhesion. J. Appl. Phys. 40 (7), 3013–3019. https://doi.org/10.1063/1.1658115.
 Dong, P., Wang, C.H., Zhao, S.Q., 2005. Preparation of high performance electro-
- Dong, P., Wang, C.H., Zhao, S.Q., 2005. Preparation of high performance electrorheological fluids with coke-like particles from FCC slurry conversion. Fuel 84 (6), 685–689. https://doi.org/10.1016/j.fuel.2004.03.021.
- Douglas, T.A., Cemazar, J., Balani, N., et al., 2017. A feasibility study for enrichment of highly aggressive cancer subpopulations by their biophysical properties via dielectrophoresis enhanced with synergistic fluid flow. Electrophoresis 38 (11), 1507–1514. https://doi.org/10.1002/elps.201600530.
- Eser, S., Wang, G., 2007. A laboratory study of a pretreatment approach to accommodate high-sulfur fcc decant oils as feedstocks for commercial needle coke. Energy Fuels 21 (6), 3573–3582. https://doi.org/10.1021/ef060541v.
- Fang, Y.J., Xiao, W.D., Wang, G.R., 1998. Study on electrostatic separation of solid-liquid system II. Measurement of saturated adsorption weight. Petrochem. Tech 27 (11), 35–40 (in Chinese).
- Freitas, C.B., Moreira, R.C., de Oliveira Tavares, M.G., et al., 2016. Monitoring of nitrite, nitrate, chloride and sulfate in environmental samples using electrophoresis microchips coupled with contactless conductivity detection. Talanta 147, 335–341. https://doi.org/10.1016/j.talanta.2015.09.075.
- Götzinger, M., Peukert, W., 2003. Dispersive forces of particle–surface interactions: direct AFM measurements and modelling. Powder Technol. 130 (1), 102–109. https://doi.org/10.1016/S0032-5910(02)00234-6.
- Greenwood, J.A., Tripp, J.H., 1967. The elastic contact of rough spheres. J. Appl. Mech. 34 (1), 153–159. https://doi.org/10.1115/1.3607616.
- Jesús-Pérez, N.M., Lapizco-Encinas, B.H., 2011. Dielectrophoretic monitoring of microorganisms in environmental applications. Electrophoresis 32 (17), 2331–2357. https://doi.org/10.1002/elps.201100107.
- Johnson, K.L., Kendall, K., Roberts, A.D., et al., 1971. Surface energy and the contact of elastic solids. Proc. Roy. Soc. Lond. A 324 (1558), 301–313. https://doi.org/ 10.1098/rspa.1971.0141.
- Li, Q., Cao, H., Qiu, Q.Z., et al., 2023. Experimental study on the removal of FCCS catalyst particles by the coupling interaction of the electrostatic field and flow field. Petrol. Sci. Technol. 41 (4), 457–476. https://doi.org/10.1080/10916466.2022.2060255.
- Li, Q., Guo, L.F., Cao, H., et al., 2021. Effects of an effective adsorption region on removing catalyst particles from an FCC slurry under a DC electrostatic field. Powder Technol. 377, 676–683. https://doi.org/10.1016/j.powtec.2020.09. 038
- Li, Q., Guo, L.F., Cao, H., et al., 2020. Microscopic mechanistic study on the removal of catalyst particles in FCCS by an electrostatic field. Powder Technol. 363, 500–508. https://doi.org/10.1016/j.powtec.2020.01.019.

- Liu, H., Jiao, S.H., Liu, W.C., et al., 2022. Effects of decompressing carbonization on the preparation of needle coke from FCC decant oil. J. Anal. Appl. Pyrolysis 162, 105454. https://doi.org/10.1016/j.jaap.2022.105454.
- Mazumder, M.K., Sims, R.A., Biris, A.S., et al., 2006. Twenty-first century research needs in electrostatic processes applied to industry and medicine. Chem. Eng. Sci. 61 (7), 2192–2211. https://doi.org/10.1016/j.ces.2005.05.002.
- Mu, M., Liu, S., DeFlorio, W., et al., 2023. Influence of surface roughness, nanostructure, and wetting on bacterial adhesion. Langmuir 39 (15), 5426–5439. https://doi.org/10.1021/acs.langmuir.3c00091.
- Naga, A., Butt, H.-J., Vollmer, D., 2021. The force required to detach a rotating particle from a liquid-fluid interface. Langmuir 37 (44), 13012–13017. https:// doi.org/10.1021/acs.langmuir.1c02085.
- Nesumi, Y., Oyama, T., Todo, Y., et al., 1990. Properties of fluid catalytic cracking decant oils of different origins in their single carbonization and cocarbonization with a petroleum vacuum residue. Ind. Eng. Chem. Res. 29 (9), 1793–1801. https://doi.org/10.1021/ie00105a009.
- Picotti, G., Borghesani, P., Cholette, M.E., et al., 2018. Soiling of solar collectors modelling approaches for airborne dust and its interactions with surfaces. Renew. Sustain. Energy Rev. 81, 2343–2357. https://doi.org/10.1016/j.rser.2017.06.043.
- Rimai, D.S., Quesnel, D.J., 2002. The adhesion of spherical particles: contributions of Van Der Waals and electrostatic interactions. J. Adhes. 78 (5), 413–429. https://doi.org/10.1080/00218460211819.
- Shevchenko, N., lakobson, O., Isakov, V., et al., 2024. Effects of particle shape and surface structure on the adsorption properties of polystyrene microplastics. Polymers 16 (22), 3159. https://doi.org/10.3390/polym16223159.
- Soltani, M., Ahmadi, G., 1999. Detachment of rough particles with electrostatic attraction from surfaces in turbulent flows. J. Adhes. Sci. Technol. 13 (3), 325–355. https://doi.org/10.1163/156856199X00668.
- Song, X.N., Liu, D., Lou, B., et al., 2018. Removal of catalyst particles from fluid catalytic cracking slurry oil by the simultaneous addition of a flocculants and a weighting agent. Chem. Eng. Res. Des. 132, 686–696. https://doi.org/10.1016/j.cherd.2018.02.016.
- Sonnenberg, A., Marciniak, J.Y., McCanna, J., et al., 2013. Dielectrophoretic isolation and detection of cfc-DNA nanoparticulate biomarkers and virus from blood. Electrophoresis 34 (7), 1076–1084. https://doi.org/10.1002/elps.201200444.
- Zhang, Z., Li, Q., Wang, Z.B., et al., 2019. Effect of structural parameters of an electrostatic separator on the removal of catalyst particles from fluid catalytic cracking slurry. Sep. Purif. Technol. 222, 11–21. https://doi.org/10.1016/j. seppur.2019.04.012.
- Zhou, T., He, X., Zhao, J., et al., 2023. Electrokinetic transport of nanoparticles in functional group modified nanopores. Chin. Chem. Lett. 34 (6), 107667. https://doi.org/10.1016/j.cclet.2022.07.010.
- Zhou, T., Ji, X., Shi, L., et al., 2020a. Dielectrophoretic interactions of two rodshaped deformable particles under DC electric field. Colloids Surf. A 607, 125493. https://doi.org/10.1016/j.colsurfa.2020.125493.
- Zhou, T., Ji, X., Shi, L., et al., 2020b. AC dielectrophoretic deformable particle-particle interactions and their relative motions. Electrophoresis 41 (10–11), 952–958. https://doi.org/10.1002/elps.201900266.
- Zimon, A.D., 1982. Adhesion of Dust and Powder. Plenum, New York. https://doi.org/10.1007/978-1-4615-8576-3.
- Zoeteweij, M.L., van der Donck, J.C.J., Versluis, R., 2009. Particle removal in linear shear flow: model prediction and experimental validation. J. Adhes. Sci. Technol. 23 (6), 899–911. https://doi.org/10.1163/156856109X411247.